The Bow Echo: Observations, Numerical Simulations, and Severe Weather Detection Methods

RON W. PRZYBYLINSKI

National Weather Service Forecast Office/NOAA, St. Louis, Missouri

(Manuscript received 13 May 1993, in final form 22 February 1995)

ABSTRACT

Bowing convective line segments (bow echoes) are often associated with swaths of damaging downburst winds and are sometimes accompanied by tornadoes that may reach violent (F4) intensity. Bow echoes range in length from less than 20 km to more than 100 km, the latter forming a broad bowing line segment. In this manuscript, both past and recent observations of bow echo convective systems will be reviewed. The meteorological environments of long-lived derecho-producing convective systems will also be presented. This will be followed by recent conceptual models and numerical simulations of bowing convective systems. Finally, the evolution of two large-scale bow echo convective systems, which produced extensive wind damage and weak tornadoes, will be described. With the ongoing installation of a comprehensive network of Doppler radars, the National Weather Service forecaster will be required to know more about conceptual storm structure models of severe convective storms. It is hoped that this literature review will result in a greater understanding of such convective systems that are often known producers of significant severe weather events.

1. Introduction

The nature of convective storm structures and their evolution have intrigued research scientists and challenged operational meteorologists since the 1950s. Of the structures that have been identified, the supercell and squall line convective storms have received the greatest attention due to the disproportionate amount of loss of life and property damage they cause. Long-lived rapidly moving convective squall line systems frequently produce widespread wind damage and large hail, and occasionally produce tornadoes. These systems often cause "multiple casualties" and seriously affect the aviation community.

Recent examples of long-lived, convective windstorms include the 7 July 1991 event over the lower Great Lakes region, the 4 May 1989 event over north-central Texas (Smith 1990), and the 28 July 1986 event over much of Iowa, eastern Missouri, and southwest Illinois (Johns and Leftwich 1988). Most of the observations and numerical research on bow echo development is limited to cases that occur during the warm season.

With the installation of WSR-88D (Weather Surveillance Radar—1988 Doppler) radar systems during the modernization and restructuring of the National Weather Service, forecasters will be required to have a strong background in mesoscale and storm-scale meteorological processes when interpreting volumetric reflectivity and Doppler velocity data. Having these data available will significantly impact the way operational meteorologists diagnose storm structure and how they warn the public for these events.

This paper will survey the research on storm structure, evolution, and radar echo patterns associated with bowing line segments within convective squall lines. An observational review of the types of echo patterns associated with convective squall lines will be followed by a brief survey of the meteorological conditions essential to the development of these systems. The introduction of conceptual models and recent numerical simulations of bowing convective systems will then be presented. This will be followed by radar observations of two derecho convective systems (case 1, the 15 June 1982 event over central and eastern Indiana; and case 2, the 19 July 1983 event over the upper Mississippi Valley region that produced surface gusts exceeding 55 m s^{-1}). It is hoped that this review will provide the operational forecaster a broad but fundamental understanding of the structural characteristics and evolution of bowing convective line segments embedded within a larger squall line system.

2. Observational Review

a. Bow echo patterns

The first observational reference to bowing convective line segments within a larger-scale convective squall line was presented by Nolen (1959). He identified an echo structure, termed "line echo wave pattern"

Corresponding author address: Ron W. Przybylinski, NWSFO, 12 Research Park Drive, St. Charles, MO 63303.

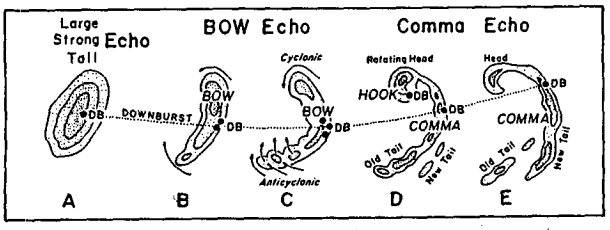

FIG. 1. A typical morphology of radar echoes associated with strong and extensive downbursts. During the period of strongest downbursts, the echo often takes the shape of a spearhead echo pointing in the direction of motion (adapted from Fujita 1978).

(LEWP) in which one part of the line segment is subjected to acceleration and an adjacent part to deceleration, resulting in a mesoscale wave pattern in the line. Nolen noted that such a wave pattern could be associated with tornadoes. About a decade later, Hamilton (1970) emphasized the significance of the bulge (accelerated portion) within the LEWP and linked this echo feature to damaging straight-line winds.

The term "bow echo" was introduced by Fujita (1978). Fujita describes the evolution of a bow echo in which downburst winds (Fujita and Caracena 1977) are the cause of the bowing in the line echo. One of the distinct characteristics of a bow echo is its linkage to very long, narrow swaths of damaging straight-line winds. The evolution of the bow echo (Fig. 1) has been categorized into three stages (tall echo, bow echo, and comma echo). During the early part of the bow echo stage intense downbursts descend from the rear flank of the tall echo, resulting in a distortion of the convective cell or line segment. During the most intense phase, the center of the bow forms a spearhead, with cyclonic and anticyclonic rotation at the ends of the bow. Rear inflow notches (RINs) along the trailing edge of the line segment usually indicate where downburst winds are the strongest (Przybylinski and Gery 1983; Burgess and Smull 1990; Wilson et al. 1980). During the dissipation stage the system evolves into a large comma-shaped echo with cyclonic (anticyclonic) rotation at the upper (lower) ends of the bow.

b. Bow echo patterns associated with derechos

Downburst-related damage patterns produced by convective wind storms were studied by Fujita and Wakimoto (1981). Their analyses revealed the existence of multiple scales of damage patterns, which were divided into five classifications (from family of downburst clusters to individual burst swaths). A family of downburst clusters extends several hundreds of kilometers, while individual burst swaths encompass tens of kilometers. On the larger end of the scale, Johns and Hirt (1987) examined a large number of warm season convective complexes that produced families of downburst clusters (which they called derechos). Johns and Hirt (1987) developed a set of criteria to identify derecho events. The criteria are the following.

(a) There must be an area of concentrated reports consisting of convectively induced wind damage and/or convective gusts greater than 26 m s^{-1} (50 kts). This area must have a major axis length of at least 400 km (250 nm).

(b) The reports within this area must also exhibit a nonrandom pattern of occurrence. That is, the reports must show a pattern of chronological progression, either as a singular swath (progressive) or as a series of swaths (serial).

(c) Within the area there must be at least three reports, separated by 64 km (40 nm) or more, of either F1 damage (Fujita 1971) and/or convective gusts of 33 m s^{-1} (65 kts) or greater.

(d) No more than 3 h can elapse between successive wind damage events.

By analyzing the radar summary charts associated with these cases, Johns and Hirt were able to identify two basic echo patterns associated with derechos. The first pattern, termed "progressive," often consists of a single bowed segment that moves parallel to a quasi-stationary front (Fig. 2a). The second pattern, referred to as "serial" consists of a series of bows and LEWPs that propagate along a large-scale squall line (Fig. 2b).

Detailed radar reflectivity structures associated with derechos occurring in the late spring and summer have been documented by Przybylinski and DeCaire (1985), Schmidt and Cotton (1989), and, most recently, Burgess and Smull (1990). Przybylinski and DeCaire (1985) identified four types of radar echo patterns from radar film records and found types 1, 2, and 3 to be the most common (Fig. 3). In the initial study, 20 derecho cases were examined from the midwest and eastern United States during the period 1980–1984. However, three additional cases were examined through 1992. Conventional radar reflectivity data within 230 km of the radar for each individual derecho event were collected using integrated log contour (VIP) presentation. For most of the cases, presentations were

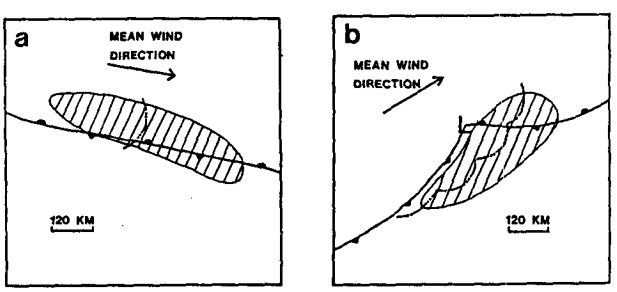

FIG. 2. Schematic presentation of features associated with (a) progressive and (b) serial derechos near the midpoint of their life cycle. Hatched area represents total area affected by damaging winds. Frontal and squall line symbols are conventional (from Johns and Hirt 1987).

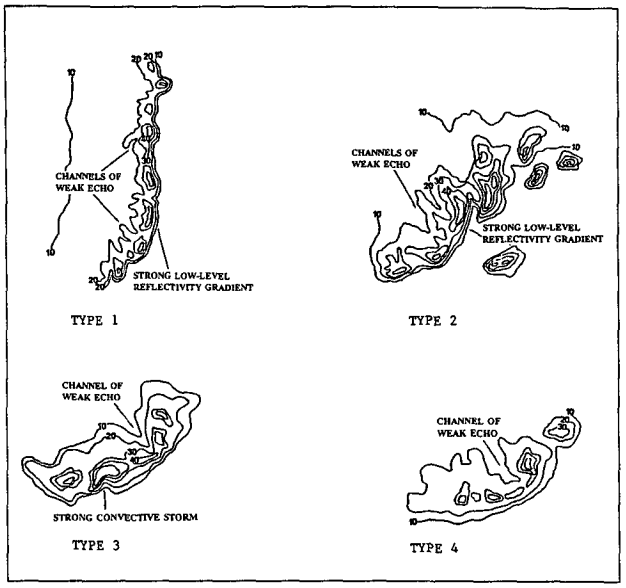

FIG. 3. Schematic diagrams of radar signatures associated with derechos. Solid lines are low-level PPI reflectivity contours (dBZ) (adapted from Przybylinski and DeCaire 1985).

compiled from plan position indicator (PPI) scans with the elevation angle set at 0.5°. However, volume scan format was completed for five derecho events; that is, the radar antenna completed revolutions at two or more step elevations.

Of the 23 cases examined, 5 cases appeared to fit the type 1 echo pattern (Fig. 3). This pattern is often characterized by two or three bowing line segments. Each individual segment may be as long as 100 km in length and may be associated with a weak mesocirculation near the comma head. A strong low-level reflectivity gradient often observed along the leading edge of the bow signifies the location of updraft centers. The maximum echo tops of individual convective elements are usually displaced over and sometimes downwind of the strong low-level reflectivity gradient. Numerous, relatively small RINs (10–15 km in width) are frequently observed along the trailing edge of each individual bowing line segment, signifying a region of evaporatively cooled-lower θ_e air being channeled toward the leading edge of the bow (Przybylinski and Schmocker 1993). The RIN structures combined with the strong low-level reflectivity gradient along the leading edge of the bow are often signals of the location where damaging downburst winds are occurring.

Seven of the cases fit the type 2 echo pattern that is characterized by a short, solid bowing convective line segment of between 80 and 100 km in length. A band of scattered to broken convective elements is associated with a surface frontal boundary or warm advection zone [warm advection wing (Smith 1990)] and typically extends downwind (eastward) from the northern end of the bulging line echo (Fig. 3). A strong low-level reflectivity gradient is observed along the leading edge of the bowing line segment, and one or more prominent RINs are noted along the trailing edge of the bow. One of the unique features of type 2 bowing convective systems is the presence of isolated convective storms downwind (east) of the predominant bow echo. These isolated convective elements often develop 50–80 km ahead of the bowing line segment and rapidly intensify as the predominant bow approaches them. Prior to merger, a strong low-level reflectivity gradient develops near the upwind (west) side of the isolated convective storm, signifying the presence of strong vertical motions ahead of the bowing line segment (Lemon 1980). A concave-shaped or ill-defined bow echo may form just after merger. In one case, over central Wisconsin, the isolated storms became parent supercells during the time of merger resulting in the formation of several strong tornadoes. In over half of the cases, tornadoes and funnel clouds were observed when merging occurred.

Nine cases have been identified with type 3 systems. Reflectivity characteristics associated with this pattern include 1) a solid bowing line segment extending between 40 and 120 km in length, 2) a strong low-level reflectivity gradient along the leading edge of the bow suggesting the location of intense updrafts, and 3) a single RIN along the trailing edge that may vary in size from 10 km to as large as 25 km in width. The radar reflectivity structure associated with the 19 July 1983 convective high wind event is a classic illustration of type 3 systems (Fig. 3). During the evolution of the bowing line segment, the size of the RIN along the trailing edge can becomes quite pronounced and increases in size. A few type 3 cases also show the transition from one bowing line segment to two or three bowing segments during the later stages of their life cycle. Scattered to broken convective storms extending downwind from the north end of the bow are occasionally observed with systems of this type.

Another unique feature of type 3 systems is the presence of one or several intense convective storms having supercell characteristics and located near the right rear flank (southwest flank) of the predominant bowing line segment. In all nine documented cases, intense convective storms produced hail (1–5 cm in diameter), funnel clouds and/or F0–F1 intensity tornadoes, and damaging winds reaching F1 intensity. In each case the intense convective storm's reflectivity structure periodically exhibited supercell characteristics. The persistence of these supercell characteristics varied from as little as 15 min to as long as 1 h, with the longevity apparently related to the depth of the vertical shear (Weisman 1991). Additionally, the intense storm often appeared to be the closest one to a stationary northwest–southeast frontal boundary. The boundary serves as a potential source of baroclinically generated horizontal vorticity and may aid in the intensification of the convective cell (Klemp 1987). Other studies have

shown that intense convective cells or supercells often intensify when intersecting with preexisting boundaries (Maddox et al. 1980; Weaver and Nelson 1982; Przybylinski et al. 1993). Schmidt and Cotton (1989) also documented a similar echo configuration during a bow echo–type event during the Cooperative Convection Precipitation Experiment experiment.

Only two cases in this sample fit the type 4 radar echo pattern shown in Fig. 3. The storm reflectivity characteristics are initially identified by an intense storm evolving through the classic high-precipitation (C-HP) supercell life cycle documented by Moller et al. (1990). During the HP evolution, new storms rapidly form 50 and 120 km south and west of the supercell. Many of these storms develop rapidly along the leading edge of the supercell's rear flank downdraft. Gradually, the supercell evolves into a bow echo structure with the mesocirculation identified within the comma head of the bow. A nearly solid line echo pattern extends upwind (south and west) of the predominant bow echo structure. Strong low-level reflectivity gradients form along the leading edge of the bowing line segment, while one or several RINs are noted along the system's trailing edge.

c. *Bow echoes associated vortices, including tornadoes*

The cases examined by Przybylinski and DeCaire (1985) suggest that the existence of either a large single RIN or numerous small RINs on the trailing edge of the stronger reflectivity cores are common elements of warm season derecho-producing convective systems. The RINs may be related to the location of midlevel rear-inflow jets and subsequently to the strongest straight-line winds within the large-scale derecho-producing system. Recent studies of severe convective windstorms using Doppler radar observations (Burgess and Smull 1990; Przybylinski and Schmocker 1993) have shown that meso- and storm-scale vortices were observed near the northern end of a rapidly moving convective squall line, while one or several RINs existed along the trailing edge of the line echo prior to the bowing of the line segment (Figs. 4a,b). In Burgess and Smull's case, the larger vortex was approximately 100 km in diameter, while the smaller circulation was a mesocyclone of 10 km in diameter. A closer inspection of the Doppler velocity presentation indicates three regions of enhanced shear along the leading edge of the outflow boundary (B, C, and D) (Fig. 4c). These intense shear regions appear to be associated with the locations of transient tornadoes. The larger of two RINs located near the northern end of the bowing line segment became more pronounced with time and it distorted the bowing line segment, while the second RIN, farther south, lost its identity. Doppler velocity data showed that the northern RIN was linked to the rear-inflow jet (RIJ) that produced outflow ground-relative

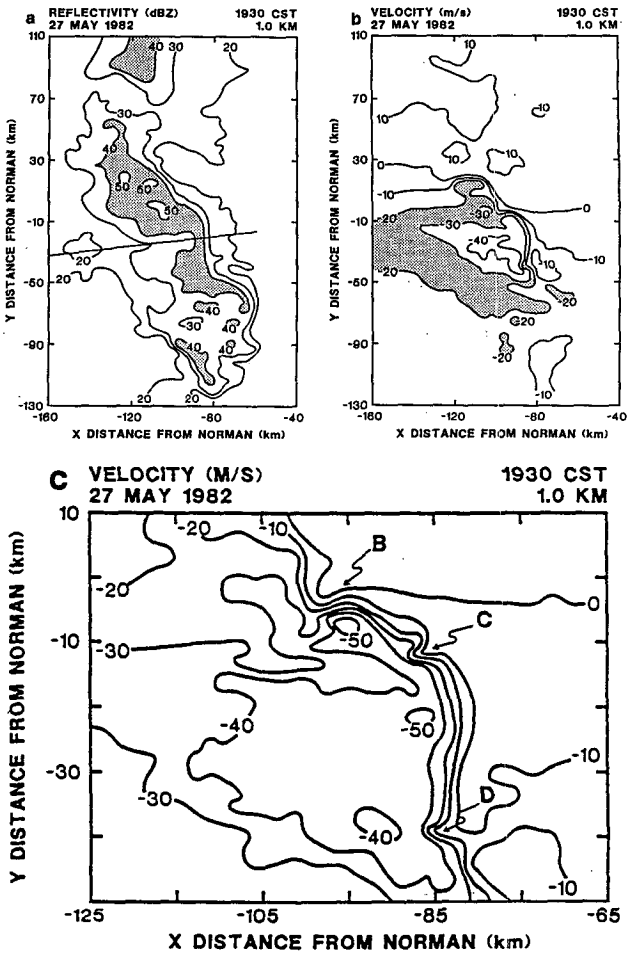

FIG. 4a. Norman, Oklahoma, single-Doppler analysis of (a) reflectivity (dBZ) and (b) low-resolution velocity (m s^{-1}) for 1930 CST 28 May 1982, at 1 km above ground level (AGL, from Burgess and Smull 1990). (c) Norman single-Doppler analysis of high-resolution velocity (m s^{-1}) data for 1930 CST 28 May 1982, at 1 km AGL (from Burgess and Smull 1990).

winds of 40 m s^{-1} at a height of 1 km. As the convective squall line further matured, other RINs were identified along the trailing edge of the bowing line segment and were linked to regions of strong outflow.

Przybylinski and Schmocker's (1993) investigation of the 2 July 1992 convective windstorm event revealed the growth of a mesovortex near the northern end of a rapidly moving convective squall line. The circulation's early stage satisfied the criteria to be called a mesocyclone (Burgess 1976), where the vortex diameter was less than 5 km and shear value exceeded 5.0 $\times 10^3$ s^{-1}. However, the circulation's diameter exceeded 15 km during the system's later stages. Similar to Burgess and Smull's case, enhanced shear regions were identified with the 2 July 1992 event north of the apex of the bow and along the northern end of the larger bowing line segment. The greatest degree of wind

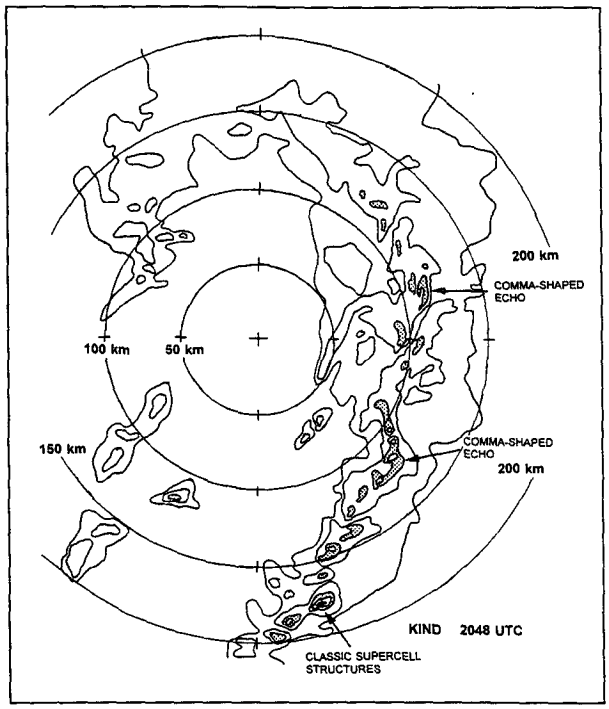

FIG. 5a. Indianapolis, Indiana, reflectivity analysis for 1548 EST 10 March 1986 at 0.5° elevation slice (from Przybylinski 1988).

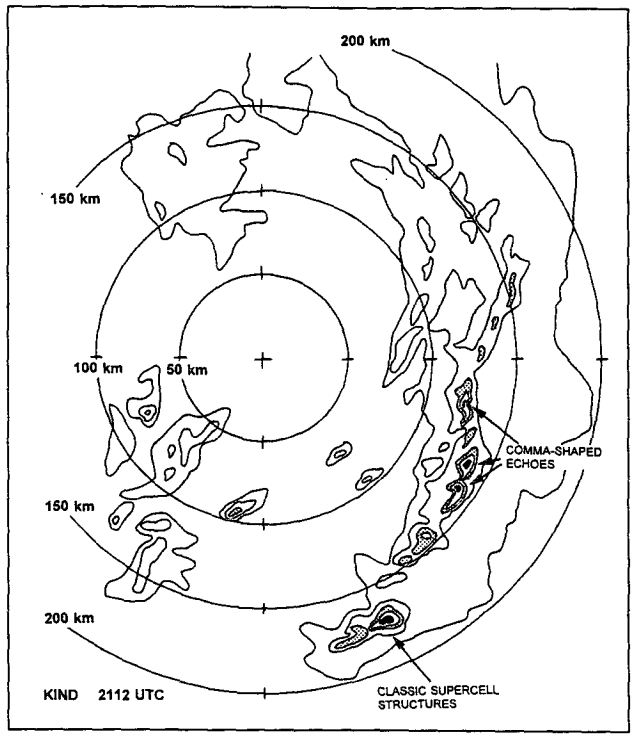

FIG. 5b. Indianapolis reflectivity analysis for 1612 EST 10 March 1986 at 0.5° elevation slice (from Przybylinski 1988).

damage and locations of transient tornadoes were linked to the location of these shear regions.

In his conceptual model, Fujita showed that bow echoes vary in length from 20 to 120 km. This scale of length appeared to apply to most bow echo systems. Most of Fujita's studies focused on the evolution of bowing structures during the warm season–weak dynamic forcing environments. Studies conducted by Wakimoto (1983) and Przybylinski (1988) have shown that in cool-season strong-dynamic environments, small-scale bow echoes of less than 20 km in length and embedded within a larger squall line can be significant wind and tornado producers. The rapidly moving extensive squall line is often associated with a "dynamic" synoptic pattern, described by Johns (1993) as one in which LEWPs typically move along the line as it progresses. In some cases the small-scale bow echoes embedded within the line can be considered as a variation of the HP supercell family, in which the parent tornado-producing circulation is located within the comma-head portion of the bow (Moller et al. 1990; Przybylinski et al. 1993). Tornadoes reaching F4 intensity have been linked to the comma-head portion of these signatures (Wakimoto 1983; Przybylinski 1988; Smith and Partacz 1985), while damaging downburst winds have occurred along the leading edge and within the vicinity of the single RIN. The RIN is a reflection of the storm's rear flank downdraft where lower θ_e air is channeled toward the leading edge of the bow.

A classic illustration showing the evolution of small bow and comma-shaped echoes associated with a cool season derecho event is the 10 March 1986 tornadic and damaging wind outbreak that occurred over parts of Indiana, northern Kentucky, and southwest Ohio. PPI reflectivity presentations at 2048 UTC (Fig. 5a)

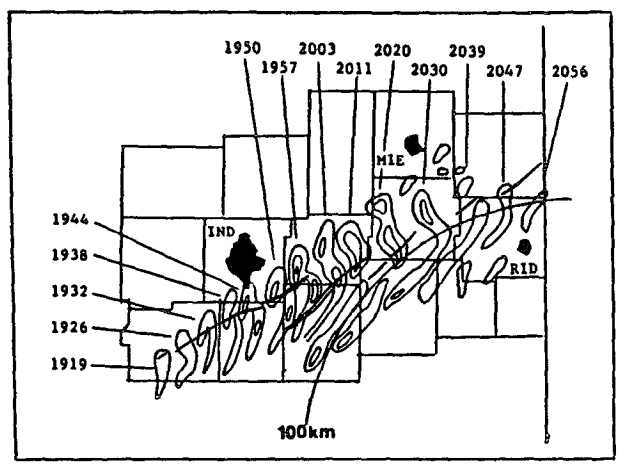

FIG. 5c. Time sequence of low-level PPI reflectivity data from Cincinnati radar on 10 March 1986. Reflectivity contours are 41 and 46 dBZ and time in UTC. Heavy solid contours represent tornado tracks. IND signifies Indianapolis. RID signifies Richmond, Indiana. MIE signifies Muncie, Indiana (from Przybylinski 1988).

and 2112 UTC (Fig. 5b) illustrate the variety of tornadic echo structures that can exist within a single convective squall line. During this period small comma-shaped echo structures, of less than 20 km in length, were observed across central sections of a larger squall line, while isolated classic and HP supercells were present near the southern end of the squall line. Tornadoes ranging from F2 to F3 intensity occurred near the comma head of the small comma-shaped echoes or near the right rear flanks of the classic supercells. Damaging downburst winds were common within the apex of the bowing structure, immediately south of the small rotating comma head and within the vicinity of small bowing line segments embedded within the larger squall line. Both tornadoes and clusters of damaging downburst winds were occurring simultaneously throughout the event.

Such variations in the tornadic echo signatures likely reflect differences in the environmental conditions ahead of the line. This includes the varying degrees of Convective Available Potential Energy (CAPE) and the nature of the vertical wind shear profile (Weisman and Klemp 1984). More importantly, this case and others (e.g., Wakimoto 1983) show that in strong shear–low CAPE environments strong and violent tornadoes (F2–F4 intensity) can be linked to a variety of storm reflectivity structures and not just to the classic supercell structures. Figure 5c shows a time sequence of one small comma-shaped echo (south and southeast of Indianapolis) embedded within the rapidly moving convective squall line on 10 March 1986 over central Indiana. As the storm deviated to the right, the strongest tornadic activity (F2–F3) occurred within the region of the comma head between 1938 and 1950 UTC. Two other weaker tornadoes (F1 intensity) occurred along the leading edge of the bowing structure, south of the comma head. These tornadoes likely resulted from strong horizontal shears and shearing instabilities along the leading edge of the bow. These findings are similar to observations documented by Forbes and Wakimoto (1983), where numerous nonmesocyclone tornadoes occurred along the leading edge of a intense bowing structure.

Observational research over the past 15 years has demonstrated that a scaling problem exists today in defining convective high wind events. The large-scale bow echoes, the small-scale bows, and RINs are all important features existing on different scales, and sometimes all may be present during a particular event. It is important for the warning forecaster to recognize that damaging outflows may be occurring on several scales within the larger squall line. The small-scale bow echoes are frequently related to local intense outflows from a single storm. In contrast, the large-scale bow echoes consisting of numerous storms may produce a broad swath of damaging winds. Additionally, RINs of varying sizes may exist on the trailing edge of large and small bowing segments. However, in spite of the difference in scales, all bow echoes contain the same structural quality: 1) a bowing line segment, and 2) RINs located at the trailing edge of the storm's reflectivity field within the area of greatest bowing.

3. Meteorological environments

Past research from a number of investigators has shown that individual bow echoes and bowing line segments can form in a wide variety of environments (Johns 1993). Embedded bowing structures within squall lines can occur any time of the year and are associated with particular synoptic patterns and parameter values. During the cool season (October–April), common reflectivity signatures include small-scale bowing structures. However, the smaller-scale mesoscale convective system (MCS)–type bow echo evolutions are generally observed during the late spring through summer seasons.

Johns and Hirt (1987) have documented the environmental conditions associated with derechos producing bow echo systems east of the Rocky Mountains occurring during the warm season (May–August). Johns and Hirt discovered that one of the most significant attributes of the warm season derecho environment is the extreme convective instability owing to high values of low-level moisture. Johns et al. (1990) found that CAPE in the genesis region of 14 intense, long-lived progressive derechos averaged 2400 J kg^{-1}. They also found that the average maximum CAPE (usually occurring near the midpoint of the derecho track) was 4500 J kg^{-1}, with a range from 2600 to 6300 J kg^{-1}. Surface dewpoints of 20°C were common. The extreme instability appears to be directly related to the pooling of low-level moisture along a thermal boundary (see Fig. 6).

The most common upper-flow pattern associated with warm season derecho-producing bow echo systems is northwesterly (Johns and Hirt 1987). At 500 mb a short-wave trough approaches the genesis region. Warm advection maxima are present near the genesis region at both 850 and 700 mb, with progressively weaker warm advection indicated to the east along the derecho track (Johns et al. 1990). Except near the genesis region, winds at 850 mb blow parallel to the upper-level winds and to the path of the derecho. Such derechos gradually move into a "classically" more unfavorable wind pattern where the wind fields are nearly parallel and/or weaken. Over 80% of the convective systems began along or north of an east–west quasi-stationary frontal boundary and then moved along the boundary. Johns and Hirt (1987) suggested that a number of factors, including 1) enhanced low-level convergence, 2) enhanced instability, and 3) enhanced low-level vertical shear, aid in the development and maintenance of a derecho-producing convective system.

A second basic synoptic pattern associated with bow echo development was termed the dynamic pattern

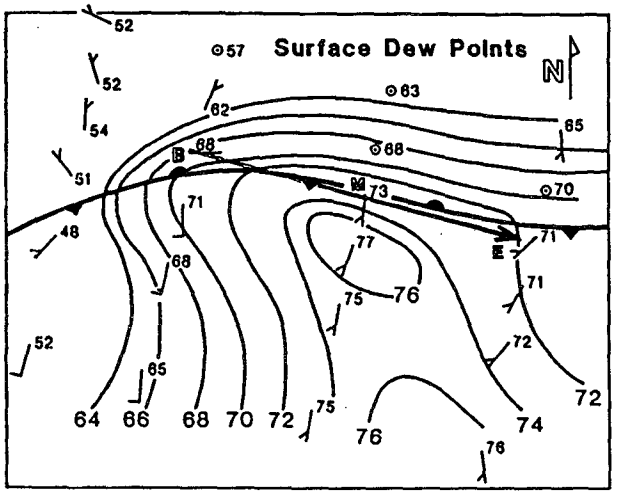

FIG. 6. Composite surface pattern for near the time of initiation of 14 long-track derechos. Dewpoint in °F and mean wind barbs in kt are plotted. Solid lines are selected isodrosotherms (from Johns et al. 1990).

(Johns 1993). This pattern is typically associated with a strong, migrating low pressure system and has many characteristics of the "classic" Great Plains tornado outbreak pattern. However, studies from Duke and Rogash (1992) showed that in the dynamic pattern the low-level jet is usually more parallel to the mid- and upper-level jets. The environmental winds associated with this type of pattern are stronger than those with the "warm season" pattern, particularly in the fall through early spring. Airmass instability can vary widely with extreme instability from late spring and summer to marginally unstable conditions in the cooler season. Johns (1993) noted that the dynamic synoptic pattern can occur anytime of the year but that the pattern was most prevalent during the cool season. This synoptic pattern is most common over the lower Mississippi Valley and southeastern states. However, the maximum frequency of occurrence shifts northward across the north-central and northeastern states during the summer.

4. Conceptual models and numerical simulations

To aid operational meteorologists in understanding the evolution of bow echoes, it is essential they understand the conceptual models and results of numerical simulations concerning these convective systems. This understanding should result in forecasters 1) acquiring a stronger knowledge base concerning the evolution and physical structure of these systems, and 2) improving their capabilities of forecasting and warning for such events.

During the PRE-STORM experiment, detailed studies conducted by Smull and Houze (1987) documented the presence of two mesoscale storm-relative airflows within MCSs that produce a bowing convective squall line. These mesoscale circulations were identified as 1) the descending mesoscale rear-inflow jet and 2) ascending front-to-rear flow. Figure 7 shows the conceptual model of the radar reflectivity and the two mesoscale flows associated with an MCS (after Houze et al. 1989). Smull and Houze observed a notchlike cavity within the trailing stratiform precipitation region of squall lines that was colocated with a descending mesoscale rear-inflow jet. This jet profoundly influenced the shape, intensity, and propagation of the leading convective line. In some cases, reflectivity and Doppler velocity data indicated that the mesoscale rear-inflow current merged with outflow from individual convective downdrafts associated with the leading convective squall line. The convective squall line's reflectivity structure (Fig. 4) illustrates this process in which one or more RINs evolve near the leading convective squall line's trailing edge. Immediately above the mesoscale rear-inflow branch lies an opposing branch of front-to-rear relative flow. Doppler observations from the PRE-STORM experiment have shown that this current originates ahead of the squall line and deepens and strengthens as it passes through the zone of deep convection. This branch continues rearward and upward into the trailing stratiform region.

Recently, Weisman (1992, 1993) has offered new insights into the evolution and mesoscale airflow structure of large-scale bow echoes through numerical modeling of such storms. These simulations result in a bow-shaped segment of convective cells with either an intense elevated or gradually descending rear-inflow jet structure located behind the apex of the bow. Cyclonic and anticyclonic eddies were located on the northern and southern ends of the bowing structure, respectively.

Using the Klemp and Wilhelmson (1978) numerical cloud model, Weisman (1992) used varied shear con-

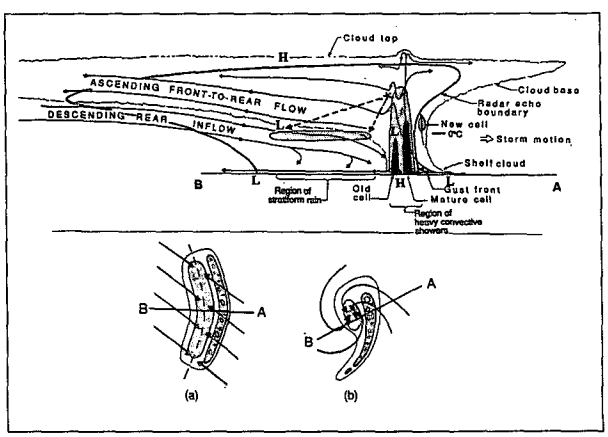

FIG. 7. Conceptual model of a squall line with a trailing stratiform area viewed in a vertical cross section oriented perpendicular to the convective line (i.e., parallel to its motion) (from Houze et al. 1989).

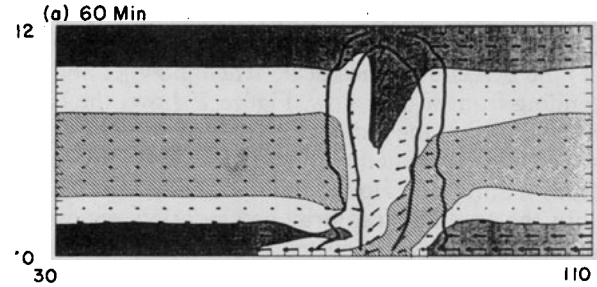

FIG. 8. Vertical cross section of θ_e flow vectors (approximately storm relative), and rainwater concentration along the y = 0 boundary at 60 min for the strong shear simulation. Vectors are presented at every other grid point, with a vector length of two grid intervals being equal to a magnitude of 25 m s^{-1}. A domain speed of u = 25 m s^{-1} is subtracted from the flow field. Regions of θ_e greater than 326 K are lightly shaded. Thick lines represent the 0 and 4 g kg^{-1} rainwater contours. Only an 80 × 12 km portion of the domain is presented (from Weisman 1993).

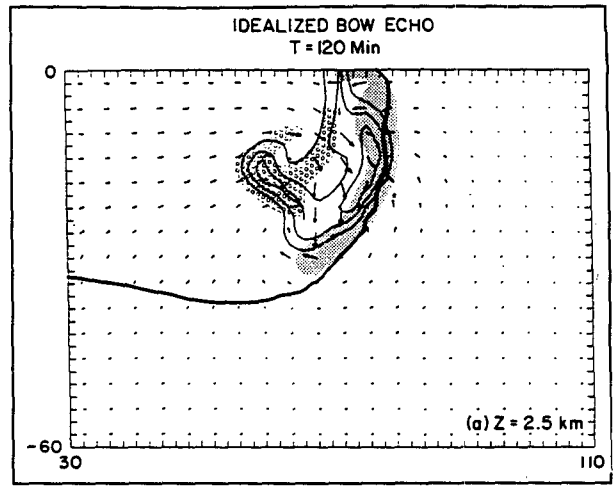

FIG. 9. Horizontal cross section of rainwater concentration and flow vectors (storm relative) at 2.5 km AGL at 120 min for an idealized bow echo simulation. Vectors are presented at every other grid point, with a vector length of two grid intervals being equal to a magnitude of 25 m s^{-1}. Rainwater is contoured at 2 g kg^{-1} intervals. Regions of updraft greater than 4 m s^{-1} are shaded, and the thick line represents location of surface gust front. Only a 60 × 80 km portion of the full domain is presented (from Weisman 1993).

ditions but held CAPE constant in producing two simulations of bowing line segments. The initial conditions for the strong shear experiment included a CAPE of 2400 J kg^{-1} and vertical wind shear of 25 m s^{-1} over the lowest 2.5 km AGL. The shear profile was linear. In contrast, for the moderate shear case, CAPE was held again constant (2500 J kg^{-1}), while the vertical wind shear was lowered to 15 m s^{-1} over the lowest 2.5 km.

In both the moderate and strong shear cases, the initial phase of the convective system's evolution is nearly identical. Weisman (1992) has shown that during the early stages the cold pool is generally weak and the ambient shear overwhelms this circulation and results in convective towers that tilt downshear (Fig. 8). As the cold pool strengthens, strong upright convective cells are noted along the leading edge of the cold pool. This process results from a balance between the system's cold pool and ambient shear. By 120 min into the simulation the cold pool further strengthens and overwhelms the ambient shear, resulting in convective towers to tilt upshear and weaken.

In the strong shear simulation, a 60-km-long bow-shaped echo forms at 120 min into the simulation with ground-relative winds reaching 40 m s^{-1} at 2.5 km (Fig. 9). Cyclonic and anticyclonic vortices having diameters of about 30 km evolved on the northern and southern ends of the bowing segment, respectively. These features, termed by Weisman (1990) as bookend vortices, appear to play a fundamental role in amplifying the rear-inflow jet and concentrating and deepening the cold pool behind the bowing line segment. The enhancement of the flow between the vortices can be interpreted as a focusing effect of the vortex couplet.

At this time (120 min into the simulation), Weisman noted that a plume of high θ_e air extends from near the surface through the entire vertical extent of the storm, while low θ_e air is beginning to descend from midlevels rearward of the convective system (Fig. 10). Strong θ_e gradients are noted between the two opposing flows. Between 120 and 180 min, the system continues to expand in size with the rear inflow strengthening considerably and extending rearward nearly 40 km from the leading edge of the system. A strong and erect updraft and rain cell is evident at the leading edge of the gust front. The core of the rear-inflow jet remains about 2.5 km AGL as it penetrates to near the leading edge of the gust front before being diverted upward and downward as it collides with the updraft current. Potentially cold midlevel air that supplies the downdraft and surface outflow circulation now feeds entirely from the rear of the convective system, in association with the rear-inflow jet. The cold pool increases in depth to nearly 3 km at the leading edge. The updraft at the leading edge of the system is still vertically erect through 5.5 km but is much stronger at lower levels than earlier. Above 5.5 km much of the high θ_e updraft

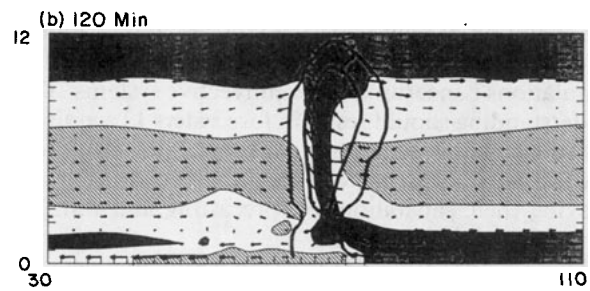

FIG. 10. Same as Fig. 8 except at 120 min (Weisman 1993).

current turns abruptly rearward (upshear). Weisman emphasized that in the strong shear case the rear-inflow jet remains elevated as a result of strong buoyancy gradients that form due to the updraft plume spreading rearward over the cold pool. The basic system by 180 min consists of 1) bookend vortices, 2) an elevated rear-inflow jet, and 3) a strong, erect updraft through 6 km along the system's leading edge.

Between 180 and 240 min, the rain field has expanded beyond 50 km behind the leading edge of the system with a strong front-to-rear current of high θ_e air above 5 km and a strong rear-inflow jet advecting low θ_e air from midlevels to the leading edge of the convective system (Fig. 11). More isolated strong convective cells are noted near the ends of the bow. The strong rear-inflow continues to remain elevated at 2–3 km near the system's leading edge, resulting in strong upright convective elements along the system's leading edge.

Weisman has noted that during the convective system's life cycle (strong shear case) the cold pool circulation will often briefly overwhelm the ambient shear, resulting in several periods where convective towers along the leading edge will briefly tilt upshear. However, the presence of a strong ambient shear will negate this process, keeping convective towers along the leading edge vertically upright. It is likely that during periods of upshear tilt damaging downburst winds are most frequent.

This structure remains in a quasi-steady state through 330 min into the simulation. The basic convective structure consists of 1) a 50-km continuous bowing segment between the bookend vortices, 2) an elevated rear-inflow jet, and 3) strong and erect updrafts through 6 km along the leading edge of the bow. These simulations indicate that the development of an organized deep convective system having an elevated mesoscale RIJ is strongly enhanced by the presence of large amounts of CAPE and strong vertical shear in the lower portions of the atmosphere. However, our understanding of long-lived convective high wind events that occur in low-instability, strong-dynamic environments is still incomplete. Additional observations and numerical modeling research must be performed to help identify the conditions that promote growth and maintenance of such convective systems.

In the weak-to-moderate shear case at 120 min, the updraft portion of the circulation has become tilted upshear, with both the original and new convective cells having weakened and advected rearward relative to the leading edge of the surface cold pool (Fig. 12a). Low θ_e air from midlevels feeds into the cold pool from the rear of the system, further strengthening and spreading the rear-inflow current along the surface. This circulation continues to expand and intensify. At 180 min into the simulation the convective system is composed of a broad, gradual ascending updraft current, extending rearward above the cold pool, and a rear-

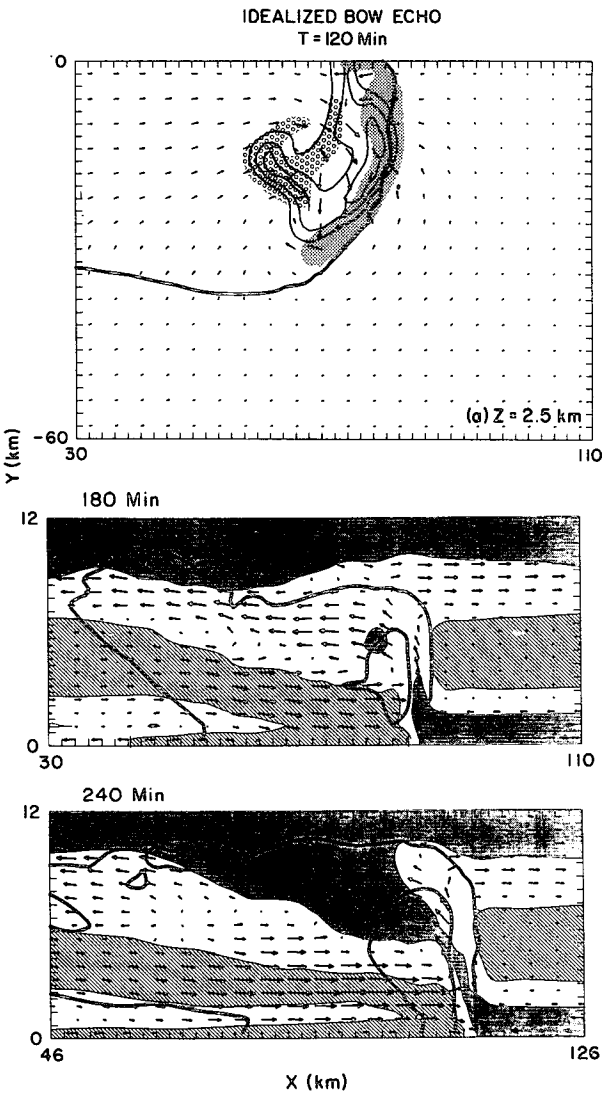

FIG. 11. (a) Same as Fig. 9 except for 180 min. (b) Same as Fig. 8 except for 180 min. (c) Same as Fig. 8 except for 240 min (from Weisman 1993).

inflow current, descending and spreading along the surface well behind the leading edge of the gust front. The lifting at the leading edge of the gust front continues to become more shallow, with scattered convective cells located well behind the leading edge of the gust front (Fig. 12b). Buoyancy gradients aloft in weak-to-moderate shear cases are less than those associated with the rearward portion of the cold pool. In contrast, the strong shear simulation showed that buoyancy and buoyancy gradients associated with the buoyant plume aloft are equal or greater in magnitude than those associated with the rearward portion of the cold pool. Thus, an elevated rear-inflow jet is produced.

Weisman (1992) conducted a number of experiments using a wide range of CAPE and ambient vertical

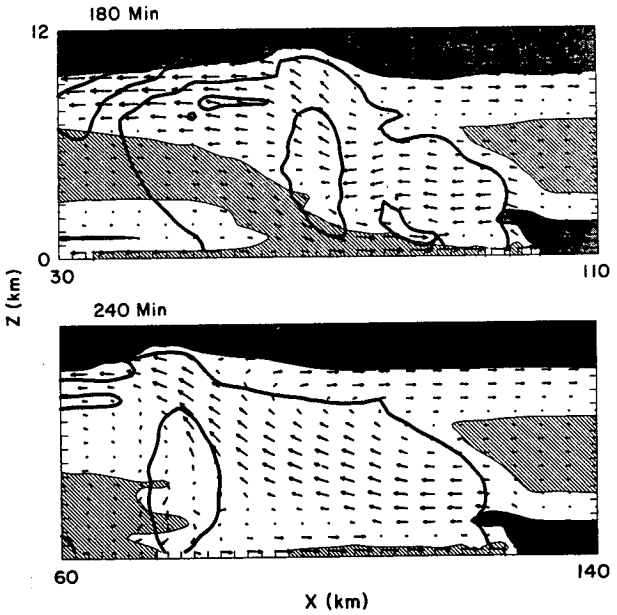

FIG. 12. (a) Same as Fig. 8 except for moderate shear simulation at 120 min. (b) Same as Fig. 8 except for moderate shear simulation at 180 min (from Weisman 1992).

wind shears to better understand the mechanisms that control the generation of the midlevel rear-inflow jets and their influence on the convective system. From these results, a range of convective structures will evolve once a rear-inflow jet becomes established. Figure 13 shows the idealized convective systems characterized by rear-inflow jets that either gradually descend and spread along the surface well behind the leading edge of the system or remain elevated to near the leading edge of the system. The strength and structure of these rear-inflow jets is controlled by the magnitude of the horizontal buoyancy gradients that are produced along the back edge of the rearward-expanding convective system. In general, Weisman (1992) noted that the rear-inflow strength increases from both increasing CAPE and increasing vertical wind shear. CAPE controls the maximum amount of buoyancy that can be realized by a parcel lifted from near the surface, while vertical wind shear controls the characteristics of the lifting produced near the leading edge of the system. The simulations Weisman (1992, 1993) has shown are controlled in very simplified environmental conditions. Future experiments, including the inclusion of ice processes and the affect of the Corolis force, will be needed to understand better the evolution of the mesoscale airflow structures and convective structures.

5. Examples of bowing convective systems

To illustrate the character and evolution of radar echo structures associated with severe convective windstorms occurring in warm season pattern environments, a time sequence of the PPI reflectivity field for two cases will be presented. Both events exhibited a broad bowed line echo structure greater than 60 km in length, with RINs along the trailing edge of the bowing segment. Clusters of damaging downburst winds, small tornadoes, and hail accompanied each event. Each convective windstorm event also satisfied the criteria for a derecho with damaging wind gusts exceeding 33 m s^{-1} and with a concentrated area of damage reports over 400 km in length.

a. Case 1—15 June 1982 derecho event

On 15 June 1982 a squall line formed over central Indiana during the mid- and late afternoon and moved across east-central Indiana and southwest Ohio. The mapping of wind damage reports during the early stages of this event is shown in Fig. 14. The convective system was characterized by a solid line of intense cells having several bowing line segments embedded within the larger squall line, similar to type I radar signatures.

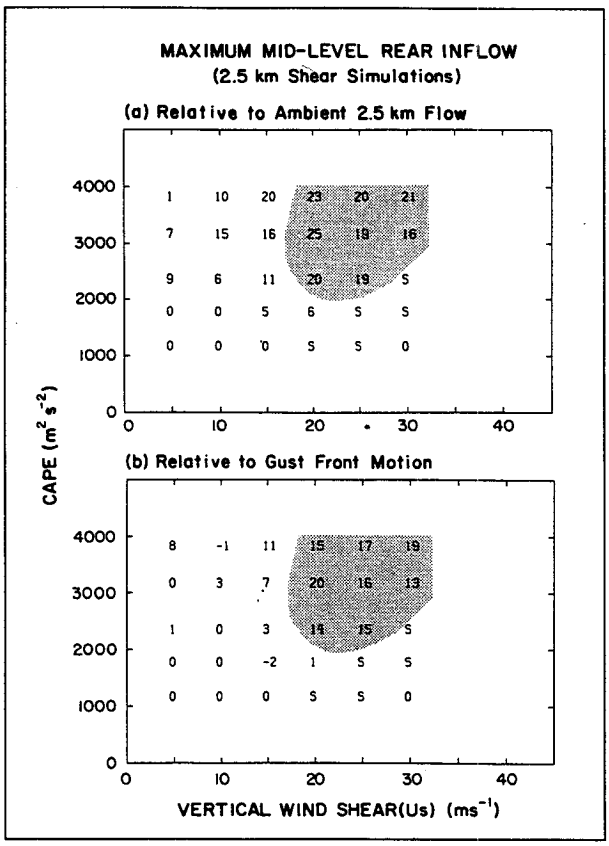

FIG. 13. Average maximum magnitude of the midlevel rear inflow (m s^{-1}) observed for the 2.5-km shear simulations between 200 and 240 min presented (a) relative to the ambient 2.5-km flow and (b) relative to the motion of the gust front. The maximum magnitude of the ambient wind for the wind profile is represented by Us. The shaded region depicts the cases that produced elevated rear-inflow jets (after Weisman 1992).

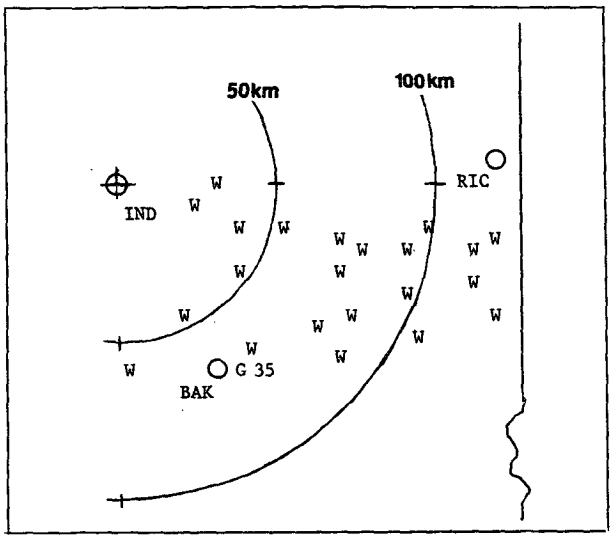

FIG. 14. Mapping of wind damage reports over central and east-central Indiana 15 June 1982. BAK represents Columbus, Indiana; RIC represents Richmond, Indiana; (W) signifies the location of wind damage reports; and (G) signifies gusts reported in m s^{-1}.

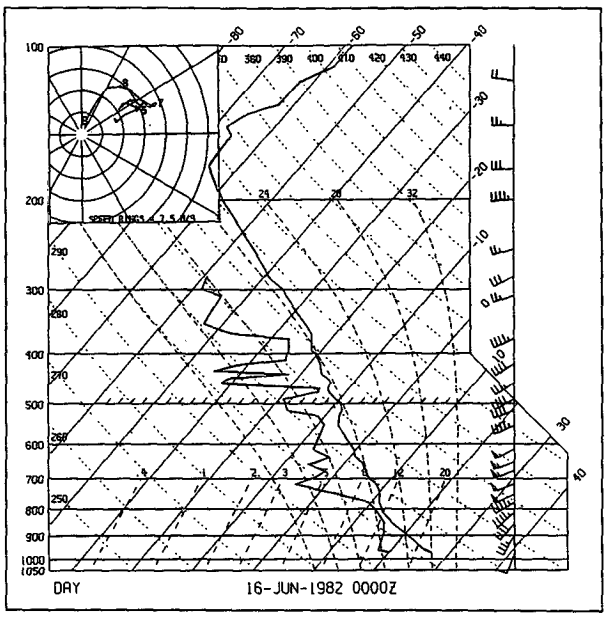

FIG. 15. Skew T–log$p$ plot of sounding from Dayton (DAY) at 0000 UTC 16 June 1982. Inset is hodograph of winds where digits (S, 8, 7, etc) mark mandatory levels (surface, 850 mb, 700 mb, etc.).

The environment ahead of the squall line was sampled by the 0000 UTC (all times UTC) Dayton, Ohio, sounding shown in Fig. 15. A moderately unstable atmosphere was present ahead of the severe squall line with CAPE values exceeding 1300 J kg^{-1}. However, the wind hodograph depicts the presence of a nearly linear shear profile with strong speed shear and slight turning of the wind within the lowest 2.0 km of the atmosphere. The Dayton sounding indicated roughly 20 m s^{-1} shear within the lowest 2.5 km. Above 2.5 km, the magnitude of the shear dropped off and the nearly linear shear profile reduced the potential for supercell formation while favoring squall line development. The magnitude of the observed low-level shear at Dayton corresponds to Weisman's strong shear simulations in which the convective squall line would have an extended life span.

The time sequence of PPI reflectivity images shown in Fig. 16 illustrates the central member of a system of three broad bowing line segments, comprising a squall line, similar to the type 1 echo pattern. An intense low-level reflectivity gradient along the leading edge of this convective line segment was evident in each of the three images. Such reflectivity gradients are very common along the leading edge since low-level convergence is maximized ahead of the line. Near the top right of each image, a weak and poorly defined comma-head echo is evident (within dashed area). The comma-head structure is characterized by intense reflectivity (50-dBZ shaded area) and a weak inflow notch near the forward edge of the comma head.

Along the trailing edge of the squall line, arrows point to the evolution of individual RINs south of the ill-defined comma-head structure. These notches increase in size with time suggesting that the mesoscale RIJ (its momentum being conserved) is penetrating into the convective cloud towers trailing side. Note that the center RIN originally begins with a hole of weaker reflectivity surrounded by high reflectivity and then gradually evolves into a larger RIN (Fig. 16). The sequence of reflectivity images appears to closely agree with Weisman's (1990) strong shear case in which the RIJ feeds low θ_e air from the rear and penetrates to near the leading edge of the storm's gust front before being diverted upward and downward as it collides with the storm's updraft plume. As each of the three bowing line segments evolved within the larger convective squall line, the central member exhibited the greatest degree of bowing. Damage survey reports indicated that the most severe wind damage was linked to the central member of the three bowing line segments and where

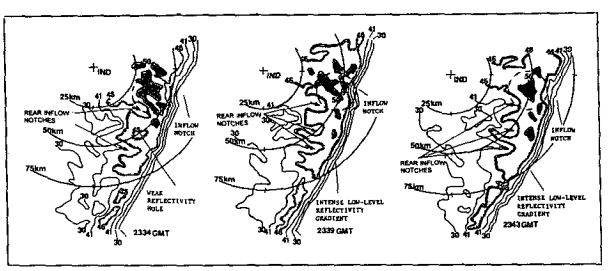

FIG. 16. Radar analysis of the derecho-producing convective system of 15 June 1982 between 2334 and 2343 UTC from Indianapolis (IND). Reflectivity contours are 18, 30, 41, and 46 dBZ. Shaded region represents reflectivity values greater than 50 dBZ.

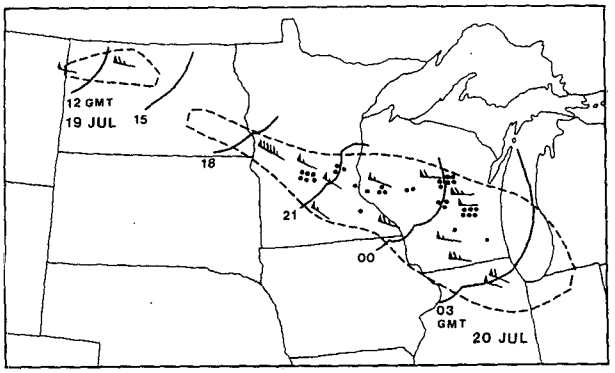

FIG. 17. Area affected by widespread downburst activity during derecho occurrence of 19–20 July 1983 (bounded by dashed line). Surface wind gusts indicated by wind flag equal 25 m s^{-1}; full barb equals 5 m s^{-1}; and half barb equals 2.5 m s^{-1}. Dots represent personal injuries. Three-hourly squall front positions indicated in UTC (from Johns and Hirt 1985).

the RINs were most pronounced (Fig. 16). Surface gusts in excess of 40 m s^{-1} were recorded within this area.

When considering the potential for damaging surface winds in type 1 convective situations, forecasters need to examine closely the PPI reflectivity data from more than one elevation angle to attempt to develop a crude three-dimensional image of the storm's structure and evolution. Reflectivity characteristics, including RINs, strong low-level reflectivity gradients along the leading edge, and bowing convective line segments are key echo features in deciding where and when to warn for damaging straight-line winds. However, as shown in this case, the bowing signature may sometimes be relatively weak. Additionally, forecasters may need to animate PPI reflectivity images to determine acceleration of bowing segments within a larger squall line. Animating a series of reflectivity images will show not only changes in the squall line composition but also movement clues associated with the squall line. Such subtle indicators can become critical in the warning decision process. As more WSR-88D radars become on line, four-panel Doppler velocity and reflectivity presentations along with animation capabilities will greatly aid the warning forecaster in diagnosing the mesoscale airflow structures, mesoscale and storm-scale circulations, and movement of bowing convective squall lines.

b. Case 2—19 July 1983 derecho event

This second case illustrates the evolution of a large-scale bowing convective system with an intense cell, possessing supercell characteristics, located along the upwind flank of the storm complex. This type 3 convective system, documented by Przybylinski and De Caire (1985), appears to be one of the more common echo patterns associated with warm season derechos.

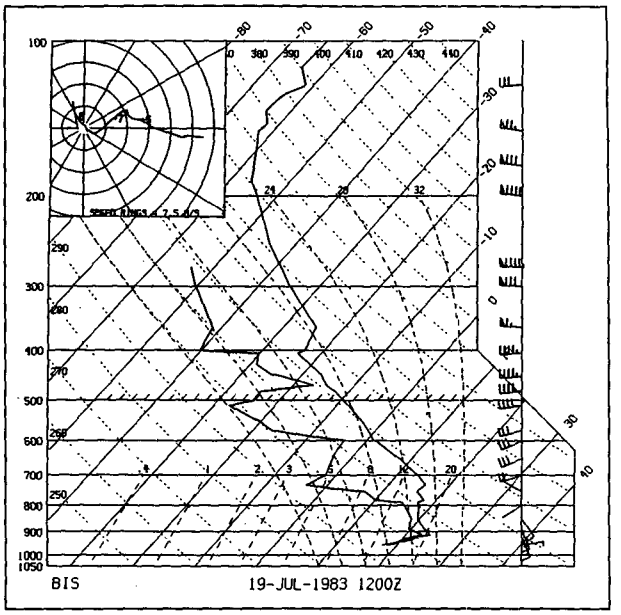

FIG. 18a. Same as Fig. 14 except for Bismarck (BIS) at 1200 UTC 19 July 1983.

During the morning of 19 July 1983 a multicellular cluster of intense storms formed over central North Dakota and moved rapidly southeastward across central Minnesota during the afternoon. The area affected by damaging winds is shown in Fig. 17. Preconvective environmental conditions were best sampled by the Bismarck, North Dakota (BIS), and Huron, South

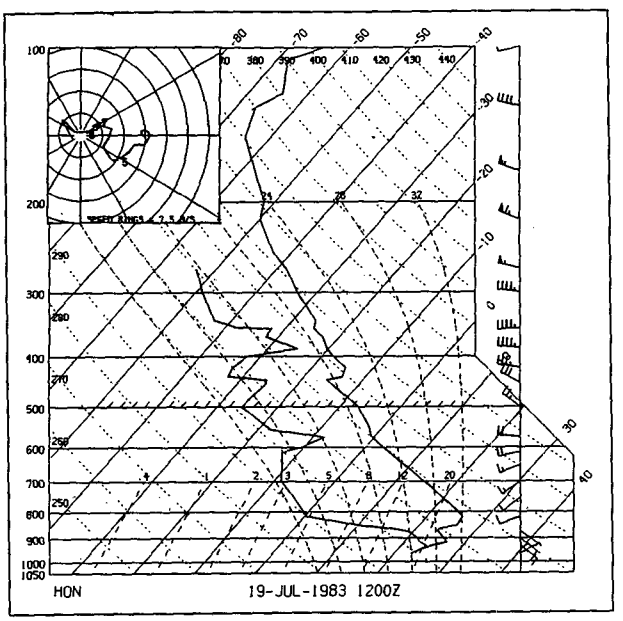

FIG. 18b. Same as Fig. 14 except for Huron (HON) at 1200 UTC 19 July 1983.

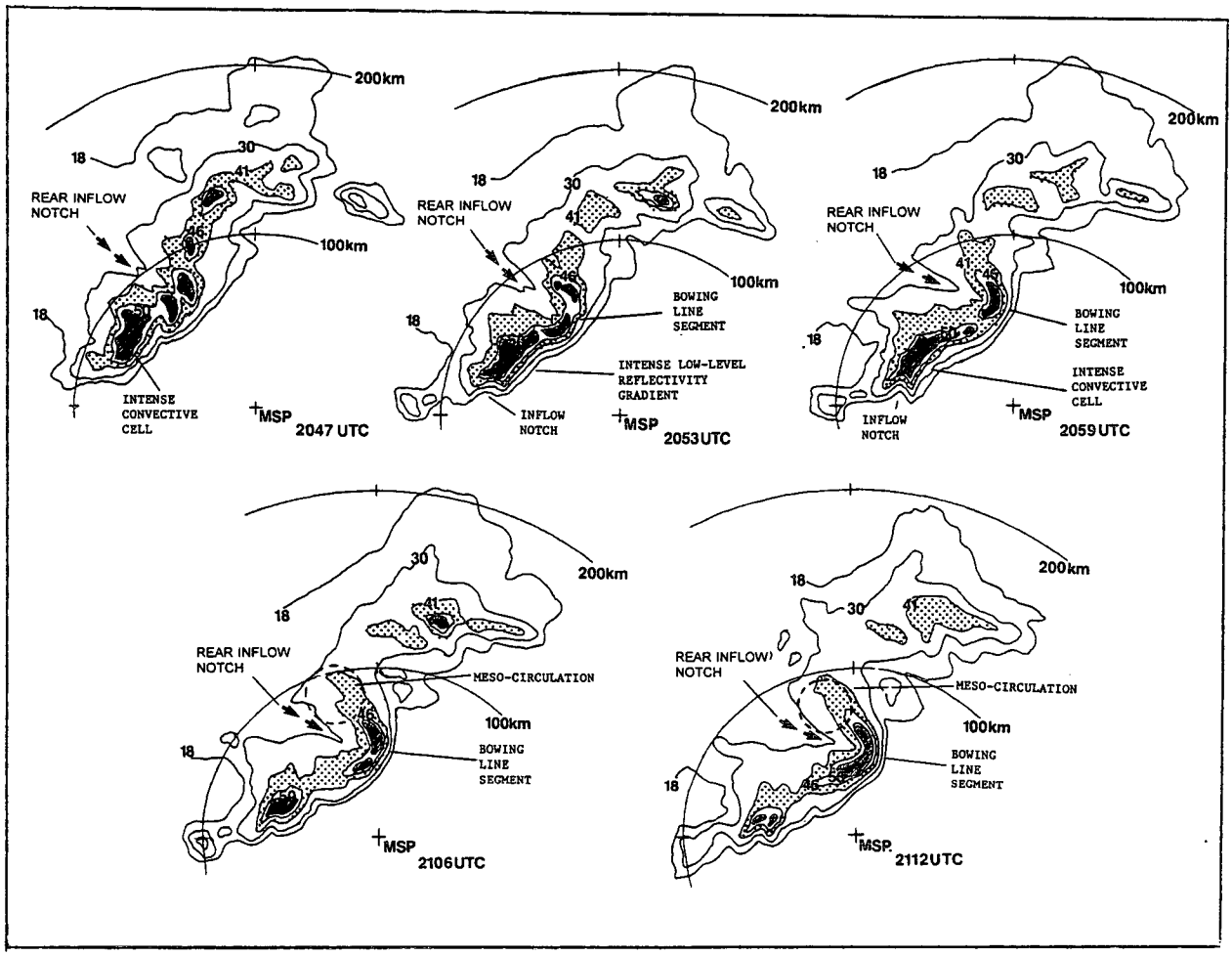

FIG. 19. Radar analysis of the central Minnesota derecho between 2047 and 2112 UTC from Minneapolis–St. Paul, Minnesota (MSP), radar. Reflectivity contours are 18, 30, 41, and 46 dBZ. Shaded region represents reflectivity values greater than 50 dBZ.

Dakota (HON), soundings at 1200 UTC (Figs. 18a,b). A moderately unstable atmosphere (CAPE $\geq$ 2100 J kg^{-1}) was present at Bismarck. The atmosphere was extremely unstable at Huron with CAPE values exceeding 3400 J kg^{-1}. Sounding data for St. Cloud, Minnesota, were not available. The wind hodographs at both sites indicate very weak shear within the lowest 2.5 km AGL and may not be representative of the near-storm wind shear environments. This is particularly so for the Huron sounding, which is south of the derecho axis and upper-level jet axis. Surface data and the Bismarck sounding suggest that a frontal inversion is present over North Dakota. In this case, one would place the base of the 2.5-km-thick layer near the top of the frontal inversion to estimate the degree of shear. Johns and Doswell (1992) have indicated in cases where convection is occurring above a frontal inversion that the inflow layer may have a base that is above the surface. Taking this into consideration, the low-level shear from above the frontal inversion at BIS would be 15 m s^{-1} (moderate shear).

PPI reflectivity images shown in Fig. 19 depict the development of a bowing line segment within a larger-scale squall line. The 2047 UTC image shows a nearly linear convective squall line with an intense convective storm, possessing supercell characteristics, near the system's upwind flank. The suggestion of a developing bowing line segment is noted northeast of the intense storm. During the next 25 min this segment rapidly accelerates southeastward with respect to the rest of the line, producing a pronounced bow echo. A strong low-level reflectivity gradient along the bowing segment's leading edge and one large RIN along the trailing flank are depicted within the bowing line segment.

At 2053 UTC the bowing line segment has intensified within the center of the squall line. The large RIN along the trailing edge of the bowing segment has become more pronounced, suggesting that the rear-inflow jet is extending rearward from the leading edge of the bowing line segment. At this time surface gusts exceeded 40 m s^{-1} near the apex of the bow. The intense storm near the southern flank continued to show su-

percell-like characteristics. This storm appeared to be close to the nearly quasi-stationary northwest–southeast boundary that extended across south-central Minnesota.

Between 2059 and 2112 UTC, the bowing line segment surged southeastward with line movement exceeding 25 m s^{-1}. The intense low-level reflectivity gradient continued along the leading edge of the bow, and the RIN became even more pronounced. These factors suggested an increase in the potential for damaging downburst winds near the apex of the bow. Damaging downburst winds exceeding 50 m s^{-1} were recorded at several airports north of the Minneapolis area. After 2100 UTC, the reflectivity pattern showed on occasion a brief acceleration of the gust front as a fine line 5–10 km ahead of the highly reflective bowing segment. The acceleration of the gust front appeared to indicate when the system's cold pool was overwhelming the ambient shear. Studies conducted by Smull and Houze (1987) and Weisman (1993) have indicated that the mesoscale rear-inflow jet structure can affect the intensity and propagation of deep convection along the system's leading edge. The gust front remained ahead of the line segment for an extended period of time after the brief acceleration. Observations during this period also indicated that several nonsupercell (F1 intensity) tornadoes occurred along the leading edge of the gust front. These nonsupercell tornadoes appeared to be similar to observations of shear vortices along convergence lines documented by Forbes and Wakimoto (1983) and Wakimoto and Wilson (1989).

The intense convective storm, near the southern flank of the convective line, significantly weakened after 2059 UTC. Przybylinski and DeCaire (1985) have documented that this type of storm evolution is typical in type 3 convective events. It is difficult to determine what factors aid in the demise of the intense convective storm. However, possible factors include 1) the shallow depth of directional and speed shear within the lowest 3 km, 2) the brief interaction with a preexisting boundary or east–west frontal boundary as documented by Johns and Hirt (1987), and/or 3) the ingestion of lower θ_e air from the convective storm's outflow (Weisman 1992; Burgess and Smull 1990).

After 2115 UTC, a large meso-β-scale cyclonic circulation developed near the northern flank of the large bowing line segment as it moved rapidly across northwest Wisconsin. An area of convective showers and thunderstorms reflecting a "warm advection wing" extended downwind from this circulation (Smith 1990). The convective bands form in an area of strong, warm advection. Weak F1 and F0 intensity nonsupercell tornadoes occurred within the region of the large mesocirculation, while significant tree and structural damage from straight-line winds and weak nonsupercell tornadoes were observed along the path of the bowing line echo. Over the next 5 h, the mesoscale convective system continued to move rapidly southeastward across Wisconsin before gradually weakening over northern Illinois and northern Indiana around 0500 UTC. Decay occurred as the system ingested negatively buoyant air from north-central Indiana that had been generated by other convection earlier in the day. A detailed mapping of the individual damage reports shown in Fig. 20 captures the degree of extensive wind damage that can be associated with strong derecho convective systems.

6. Summary

This survey attempts to aid in the understanding of the structure and evolution of bowing convective systems by providing a review of the observation of the echo patterns associated with these storms and by presenting the current conceptual models of these systems based on both observations and numerical modeling experiments. Strong low-level reflectivity gradients along the leading edge of the bow, rear-inflow notches along the system's trailing flank, and a bowing structure or segment that accelerates within a larger squall line are all important echo features that will help operational forecasters determine what areas along a squall line require severe weather warnings. However, there are still many aspects of bowing convective systems that remain unexplained and undocumented, particularly within the meso-β scale and with those cases occurring in strong-dynamic low-instability environments. Doppler radar observations and numerical modeling of bowing convective line segments have offered insights into how these systems mature. But additional radar observations, including Doppler data, from other parts of the country (outside the central and southern plains) and from other sea-

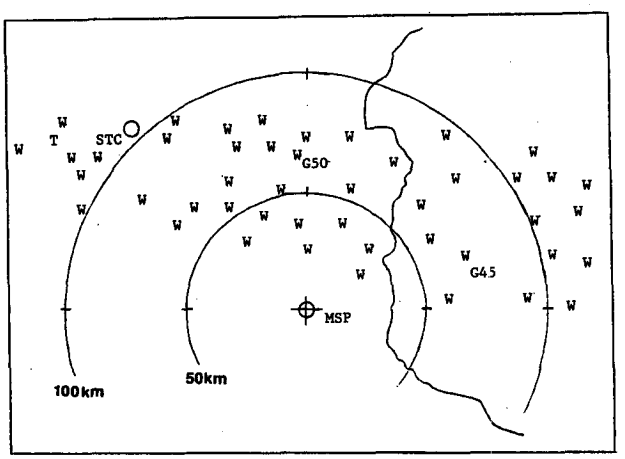

FIG. 20. Mapping of wind damage reports over central Minnesota and northwest Wisconsin 19 July 1983. STC represents St. Cloud, Minnesota; (W) signifies location of wind damage report; and (G) signifies gusts reported in m s^{-1}.

sons will be needed to update current conceptual models.

Within the last year or two, National Weather Service forecasters at several sites have been exposed to a wealth of Doppler velocity and high-resolution reflectivity data across their area of warning responsibility. The quantity and type of data presented have changed the way operational forecasters examine the atmosphere. With the increasing wealth of Doppler data available, the operational forecaster will learn more about the evolution of bowing convective systems. Proficient and trained forecasters will be needed to assimilate and apply this information properly to make skillful warning decisions. Most importantly, there will be challenges for researchers and forecasters alike to identify and understand the structure and life cycle of bowing convective systems and discover the most effective method to use these new datasets to generate accurate and timely warnings.

Acknowledgments. The author is grateful to Dr. Joseph T. Schaefer, director of the National Weather Service Training Center, and to Drs. Richard L. Livingston and Preston Leftwich, NWS Central Region Scientific Services Division, for their many beneficial suggestions on improving the manuscript. The author would also like to extend his appreciation to Dr. Brad Smull of ERL, Dr. Morris Weisman of NCAR, and an anonymous referee for their constructive comments on improving the presentation. Final thanks goes to Mr. Steve Thomas, MIC(AM) WSFO St. Louis, for his support in the preparation of the paper.

REFERENCES

Burgess, D. W., 1976: Single Doppler radar vortex recognition: Part 1—Mesocyclone signatures. Preprints *17th Conf. on Radar Meteorology,* Melbourne, FL, Amer. Meteor. Soc., 97–103.

——, and B. F. Smull, 1990: Doppler radar observations of a bow echo associated with a long-track severe windstorm. Preprints, *16th Conf. on Severe Local Storms,* Kananaskis Park, AB, Canada, Amer. Meteor. Soc., 203–208.

Duke, J. D., and J. A. Rogash, 1992: Multiscale review of the development and early evolution of the 9 April 1991 derecho. *Wea. Forecasting,* **7,** 623–635.

Forbes, G. S., and R. M. Wakimoto, 1983: A concentrated outbreak of tornadoes, downbursts, and microbursts, and implications regarding vortex classification. *Mon. Wea. Rev.,* **111,** 220–235.

Fujita, T. T., 1971: Proposed characterization of tornadoes and hurricanes by area and intensity. SMRP Research Paper No. 91, Dept. of Geophysical Science, University of Chicago, 42 pp.

——, 1978: Manual of downburst identification for project NIMROD. SMRP Research Paper 156, University of Chicago, 42 pp.

——, and F. Caracena, 1977: An analysis of three weather-related aircraft accidents. *Bull. Amer. Meteor. Soc.,* **58,** 1164–1181.

——, and R. M. Wakimoto, 1981: Five scales of airflow associated with a series of downbursts on 16 July. 1980. *Mon. Wea. Rev.,* **109,** 1438–1456.

Hamilton, R. E., 1970: A review of the use of radar in detection of tornadoes and hail. ESSA Tech. Memo. WBTM-ER-34, 64 pp. [Available from NWS Eastern Region, Scientific Services Division, Bohemia, NY 11716.]

Houze, R. A., Jr., S. A. Rutledge, M. I. Biggerstaff, and B. F. Smull, 1989: Interpretation of Doppler weather radar displays of midlatitude mesoscale convective systems. *Bull. Amer. Meteor. Soc.,* **6,** 608–618.

Johns, R. H., 1993: Meteorological conditions associated with bow echo development in convective storms. *Wea. Forecasting,* **8,** 294–299.

——, and P. W. Leftwich Jr., 1988: The severe thunderstorm outbreak of July 28–29, 1986. A case exhibiting both isolated supercells and a derecho producing convective system. Preprints, *15th Conf. on Severe Local Storms,* Baltimore, MD, Amer. Meteor. Soc., 448–451.

——, and W. D. Hirt, 1987: Derechos: Widespread convectively induced windstorms. *Wea. Forecasting,* **2,** 32–49.

——, and C. A. Doswell III, 1992: Severe local storm forecasting. *Wea. Forecasting,* **7,** 588–612.

——, K. W. Howard, and R. A. Maddox, 1990: Conditions associated with long-lived derechos—An examination of the large-scale environment. Preprints, *16th Conf. Severe Local Storms,* Kananaskis Park, AB, Canada, Amer. Meteor. Soc., 408–412.

Klemp, J. B., 1987: Dynamics of tornadic thunderstorms. *Ann. Rev. Fluid Mech.,* **19,** 369–402.

——, and R. B. Wilhelmson, 1978: The simulation of three-dimensional convective storm dynamics. *J. Atmos. Sci.,* **35,** 1070–1096.

Lemon, L. R., 1980: Severe thunderstorm radar identification techniques and warning criteria. NOAA Tech. Memo. NWS NSSFC-3, Kansas City, 60 pp.

Maddox, R. A., L. R. Hoxit, and C. F. Chappell, 1980: A study of tornadic thunderstorm interactions with thermal boundaries. *Mon. Wea. Rev.,* **108,** 322–336.

Moller, A. R., C. A. Doswell III, and R. W. Przybylinski, 1990: High-precipitation supercells: A conceptual model and documentation. Preprints, *16th Conf. Severe Local Storms.* Kananaskis Park, AB, Canada, Amer. Meteor. Soc., 52–57.

Nolen, R. H., 1959: A radar pattern associated with tornadoes. *Bull. Amer. Meteor. Soc.,* **40,** 277–279.

Przybylinski, R. W., 1988: Radar signatures associated with the 10 March 1986 tornado outbreak over central Indiana. Preprints, *15th Conf. on Severe Local Storms,* Baltimore, MD, Amer. Meteor. Soc., 253–256.

——, and W. J. Gery, 1983: The reliability of the bow echo as an important severe weather signature. Preprints, *13th Conf. on Severe Local Storms,* Tulsa, OK, Amer. Meteor. Soc., 270–273.

——, and D. M. DeCaire, 1985: Radar signatures associated with the derecho. One type of mesoscale convective system. Preprints, *14th Conf. on Severe Local Storms,* Indianapolis, IN, Amer. Meteor. Soc., 228–231.

——, and G. K. Schmocker, 1993: The evolution of a widespread convective windstorm event over Central and Eastern Missouri. Preprints, *13th Conf. on Weather Analysis and Forecasting,* Vienna, VA, Amer. Meteor. Soc., 461–465.

——, J. T. Snow, E. M. Agee, and J. T. Curran, 1993: The use of volumetric radar data to identify supercells. A case study of June 2, 1990. *The Tornado: Its Structure, Dynamics, Prediction, and Hazards, Geophys. Monogr.,* No. 79, Amer. Geophys. Union, 241–250.

Schmidt, J. M., and W. R. Cotton, 1989: A high plains squall-line associated with severe surface winds. *J. Atmos. Sci.,* **46,** 281–302.

Smith, B. E., 1990: Mesoscale structure of a derecho-producing convective system: The southern Great Plains storms of May 4 1989. Preprints, *16th Conf. on Severe Local Storms,* Kananaskis Park, AB, Canada, Amer. Meteor. Soc., 428–433.

——, and J. W. Partacz, 1985: Bow-echo induced tornado at Minneapolis on 26 April 1984. Preprints, *14th Conf. on Severe Local Storms,* Indianapolis, IN, Amer. Meteor. Soc., 81–84.

Smull, B. F., and R. A. Houze Jr., 1987: Rear Inflow in squall-lines with trailing stratiform precipitation. *Mon. Wea. Rev.*, **115,** 2869–2889.

Wakimoto, R. M., 1983: The West Bend Wisconsin storm of 4 April 1981. A problem in operational meteorology. *Mon. Wea. Rev.*, **111,** 181–189.

——, and J. W. Wilson, 1989: Non-supercell tornadoes. *Mon. Wea. Rev.*, **117,** 1113–1140.

Weaver, J. F., and S. P. Nelson, 1982: Multiscale aspects of thunderstorm gust fronts and their affects on subsequent storm development. *Mon. Wea. Rev.*, **110,** 707–718.

Weisman, M. L., 1992: The role of convectively generated rear-inflow jets in the evolution of long-lived mesoconvective systems. *J. Atmos. Sci.*, **49,** 1826–1847.

——, 1993: The genesis of severe, long-lived bow echoes. *J. Atmos. Sci.*, **50,** 645–670.

——, and J. B. Klemp, 1984: The structure and classification of numerically simulated convective storms in directionally varying wind shears. *Mon. Wea. Rev.*, **112,** 2479–2498.

Wilson, J., R. Carbone, H. Baynton, and R. Serafin, 1980: Operational application of meteorological Doppler radar. *Bull. Amer. Meteor. Soc.*, **61,** 1154–1168.